Please cite as: Falter, C., Pitz-Paal, R., "Energy analysis of solar thermochemical fuel production pathway with a focus on waste heat recuperation and vacuum generation", Solar Energy, Vol. 176 pp. 230-240, 2018. doi: 10.1016/j.solener.2018.10.042

Contents lists available at ScienceDirect

Solar Energy

journal homepage: www.elsevier.com/locate/solener

Energy analysis of solar thermochemical fuel production pathway with a focus on waste heat recuperation and vacuum generation

Christoph Falter[a,*], Robert Pitz-Paal[b]

[a] Bauhaus Luftfahrt e.V., Willy-Messerschmitt-Straße 1, 82024 Taufkirchen, Germany
[b] DLR, Institute of Solar Research, Linder Höhe, 51147 Köln, Germany

ARTICLE INFO

Keywords:
Solar fuels
Waste heat
Vacuum pumping
Efficiency

ABSTRACT

The solar thermochemical fuel production pathway as an attractive option for the decarbonization of the transportation sector is investigated. Using ceria as the reactive material and the latest published data on inert gas demand and energy demand for vacuum pumping from the literature, the energy balance of the thermochemical reactor is analyzed for vacuum pumping and inert gas sweeping, and the required process parameters for reaching high efficiencies are discussed. It is found that thermochemical energy conversion efficiencies exceeding 20% can only be reached with a vacuum operated system at reduction temperatures of 1900 K, enhanced pump efficiency by 50%, a concentration ratio of 5000 suns, and an energy recuperation effectiveness from the gases and the solid phase of 70%. We then investigate the whole fuel production pathway from incident sunlight to liquid hydrocarbons by performing an energy analysis of a fuel production plant including waste heat recovery. It is found that the energy losses theoretically can be used to cover the demand for electricity and low-temperature heat, as well as the heating of the reactants to the oxidation temperature, enhancing the pathway efficiency from 5.3% to 8.6%. The heat recovery from the single process steps along the fuel production pathway therefore has a large potential to increase the efficiency of the process, improving the economic and ecological performance significantly. Likewise, waste heat may be used to partially relax the likely stringent operating conditions of highly efficient thermochemical reactors, which could have important implications for reactor design.

1. Introduction

A countermeasure against global warming is the decarbonization of the transportation sector. While the electrification of cars is a feasible option which is thought to have the potential to replace the internal combustion engine, for aviation, on the other hand, analyses show that long-range travel is very likely to rely on hydrocarbon fuels also in the future as the specific energy of batteries is limited (Kuhn and Sizmann, 2012). To reach the ambitious goals set by the aviation industry (Air Transport Action Group, 2017) the use of alternative fuels is thus imperative. Different options exist such as the electrochemical pathway (Schmidt et al., 2016; König et al., 2015; Goldmann et al., 2018) that combines photovoltaics with electrolysis, or the photochemical pathway that uses biomass (Axelsson et al., 2012; Gollakota et al., 2018) or artificial leaves to produce hydrogen (Nocera, 2017). The solar thermochemical fuel promises high energy conversion efficiencies (Scheffe and Steinfeld, 2012; Lapp et al., 2012; Ermanoski et al., 2013; Jarrett et al., 2016) through the use of the full solar spectrum and has achieved significant efficiency advancements in the recent past (Chueh et al., 2010; Furler et al., 2012; Marxer et al., 2017). The pathway converts CO_2 and H_2O into CO and H_2 (syngas) through a redox cycle operated at high temperature using concentrated solar energy as the source of heat (Fig. 1). The material, a metal oxide, is reduced at high temperature and low oxygen partial pressure and oxidized with H_2O and CO_2 at lower temperature (Chueh et al., 2010; Romero and Steinfeld, 2012). The produced syngas is then converted into liquid hydrocarbons in the Fischer-Tropsch synthesis (FT), whereas a low-temperature synthesis yields longer-chained hydrocarbons, which are converted into chains of desired length in the jet fuel range by hydrocracking and distillation. An advantage of the solar thermochemical pathway is that the feed streams of H_2 and CO can be produced in separate reactors and therefore easily brought to the required ratio of H_2/CO of approximately two in the FT reactor.

Solar thermochemical fuels have been suggested to possess a potentially high energy conversion efficiency (Steinfeld and Epstein, 2001) and low greenhouse gas emissions (Falter et al., 2016). The

* Corresponding author.
E-mail addresses: christoph.falter@bauhaus-luftfahrt.net (C. Falter), robert.pitz-paal@dlr.de (R. Pitz-Paal).

https://doi.org/10.1016/j.solener.2018.10.042
Received 16 April 2018; Received in revised form 11 September 2018; Accepted 11 October 2018

Nomenclature

$\dot{Q}_{aux}$	auxiliary thermal power [W]
$\dot{Q}_{heat,CO_2}$	thermal power to heat CO_2 to T_L [W]
$\dot{Q}_{heat,CeO_2}$	thermal power to heat ceria from T_L to T_H [W]
$\dot{Q}_{heat,inertgas}$	thermal power for inert gas heating to T_H [W]
$\dot{Q}_{products}$	thermal power in product stream [W]
$\dot{Q}_{red,CeO_2}$	thermal power to reduce ceria [W]
$\dot{Q}_{rerad}$	thermal reradiation from reactor at T_H [W]
$\dot{Q}_{solar}$	concentrated solar power input to reactor [W]
$\dot{n}_{CeO_2}$	molar flow rate of ceria [mol s^{-1}]
$\dot{n}_{CO_2}$	molar flow rate of CO_2 [mol s^{-1}]
$\dot{n}_{O_2}$	molar flow rate of O_2 [mol s^{-1}]
$\dot{n}_{CO}$	molar flow rate of CO [mol s^{-1}]
$\dot{n}_{inertgas}$	molar flow rate of inert gas [mol s^{-1}]
$E_{inertgas}$	specific energy of inert gas production [J mol^{-1}]
h_{O_2}	specific enthalpy of oxygen [J mol^{-1}]
h_{CO}	specific enthalpy of carbon monoxide [J mol^{-1}]
h_{CO_2}	specific enthalpy of carbon dioxide [J mol^{-1}]
$P_{aux,inertgas}$	auxiliary power for inert gas reactor [W]
$P_{aux,vacuum}$	auxiliary power for vacuum reactor [W]
P_{aux}	auxiliary power input to reactor [W]
$P_{inertgas}$	power for inert gas production [W]
P_{pump}	vacuum pumping power [W]
$P_{sep,\frac{CO}{CO2}}$	power for CO/CO_2 separation [W]
T_0	temperature of surroundings [K]
T_H	reduction temperature [K]
$T_{he,end}$	temperature of ceria at the exit of heat exchanger [K]
T_L	oxidation temperature [K]
T_{pump}	temperature of vacuum pump [K]
c_{p,CeO_2}	specific heat capacity of ceria [J kg^{-1} K^{-1}]
c_{p,CO_2}	specific heat capacity of CO_2 [J kg^{-1} K^{-1}]
c_{p,CO_2}	specific heat capacity of CO_2 [J kg^{-1} K^{-1}]
c_{p,O_2}	specific heat capacity of O_2 [J kg^{-1} K^{-1}]
$c_{p,CO}$	specific heat capacity of CO [J kg^{-1} K^{-1}]
$c_{p,inertgas}$	specific heat capacity of inert gas [J kg^{-1} K^{-1}]
f_{CO_2}	CO_2 flow rate relative to stoichiometric amount [–]
p_{O_2}	oxygen partial pressure [Pa]
p_{ox}	oxidation pressure [Pa]
p_{red}	reduction pressure [Pa]
δ_{ox}	nonstoichiometry of ceria after oxidation [mol_O mol^{-1}]
δ_{red}	nonstoichiometry of ceria after reduction [mol_O mol^{-1}]
η_{abs}	absorption efficiency of solar reactor [–]
ε_{gasrec}	effectiveness of gas heat recuperation [–]
ε_{he}	heat exchanger effectiveness [–]
$\eta_{heat-to-electricity}$	efficiency of heat to electricity conversion [–]
η_{pump}	efficiency of vacuum pump [–]
ΔH_{red}	molar enthalpy of thermal reduction of ceria [J mol^{-1}]
$\mathscr{R}$	universal gas constant [J mol^{-1} K^{-1}]
C	concentration ratio of solar energy [–]
I	intensity of solar radiation [kW m^{-2}]
T	temperature [K]
δ	nonstoichiometry of ceria after reduction [mol_O mol^{-1}]

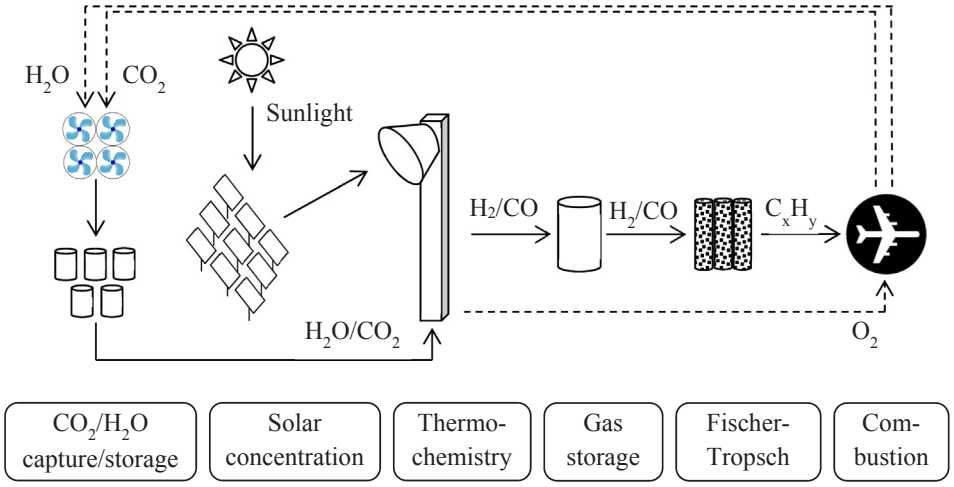

Fig. 1. Schematic representation of the solar thermochemical fuel production pathway. H_2O and CO_2 can be captured from the air and from the sea, respectively. Direct solar radiation is concentrated by a field of heliostats or dishes and enables the high-temperature thermochemical conversion of H_2O and CO_2 to H_2 and CO (syngas). The resulting syngas is stored and converted into jet fuel via the Fischer-Tropsch process.

realization of these benefits however hinges on the achievement of high efficiencies of both the thermochemical conversion and the overall fuel production pathway. For the former, values of around 20% are believed to be required to enable the large-scale economic deployment of the solar thermochemical fuel technology. The theoretical upper limit of thermochemical efficiency was shown to be well above this value for the reactive material ceria (Scheffe and Steinfeld, 2012; Chueh and Haile, 2010), depending i.a. on the level of heat recovery and the technology used for the establishment of a low oxygen partial pressure. Different reactive materials have been suggested, such as zinc oxide, ferrites, ceria, or perovskites, whereas we limit the analysis to pure ceria, which undergoes nonstoichiometric redox reactions and has shown promising experimental results recently (Chueh et al., 2010; Furler et al., 2012; Marxer et al., 2017). In nonstoichiometric redox reactions, only a small part of the material actually undergoes reduction and oxidation, while all of the material has to be thermally cycled between the reduction and oxidation temperature. Thus heat recuperation from the solid phase gains a high importance for the achievement of high efficiencies. In recent studies, counter-rotating cylinders are used to enable solid-solid heat exchange between reactive material and a heat exchange medium (Lapp et al., 2013), and between oxidized and reduced material (Allendorf et al., 2008). Potential heat exchanger effectiveness is indicated to reach values close to 70% (Lapp et al., 2013). In another analysis (Felinks et al., 2014), the multi-stage heat transfer between reactive ceria particles and inert particles is described with a potential for heat recovery effectiveness of over 70%. In a study of a generic counter-flow reactor using reactive elements of ceria that exchange heat by radiation, a similar potential for heat exchanger effectiveness was derived (Falter and Pitz-Paal, 2017; Falter et al., 2015a).

The establishment of a low oxygen partial pressure can be achieved by flushing the reduction chamber with an inert gas to dilute and remove the evolving oxygen (Chueh et al., 2010; Furler et al., 2012; Marxer et al., 2015a; Welte et al., 2016). The exact amount of inert gas which is required for a certain level of oxygen partial pressure is subject

to significantly deviating assumptions in the literature. While in a first study by Ermanoski et al. (2013) the perfect dilution of oxygen leads to very large gas flow rates and hence to quite low efficiencies, in another by Bader et al. (2013) it was assumed that in a counter-flow arrangement of ceria and gas, thermodynamic equilibrium can be reached at the inlet and outlet, leading to very low gas flow rates. In a third work eventually by Brendelberger et al. (2015) it was argued that the flow rate of inert gas has to be between these two extreme values and a function for its size is given based on the thermodynamic characteristics of the material and the oxygen uptake capability of the gas. We make use of this latest result by Brendelberger et al. to give a realistic estimate of the reactor efficiency and compare the result with the operation under vacuum. This allows a more realistic comparison of these two concepts.

In this study, we analyze the possibilities to achieve high thermochemical energy conversion efficiencies, preferably above 20%, based on a fundamental investigation of the energy balance of a solar thermochemical reactor. The two operation modes of inert gas sweeping and vacuum pumping are investigated using latest results from the literature concerning sweep gas demand and efficiency of vacuum pumping. Furthermore, we investigate which operational parameters have to be enhanced to significantly increase the efficiency. The system boundary is then widened to include the whole fuel production pathway from incident sunlight to liquid hydrocarbons, and the energy balance is presented including energy requirements and losses along the production chain. Possibilities for heat recovery are analyzed and a large potential for the increase of efficiency is found which could significantly enhance the economic and environmental performance of a solar thermochemical fuel production plant.

2. Solar thermochemical syngas production

2.1. Energy balance

In the analysis of the solar thermochemical redox cycle below, we limit the study to CO_2 splitting, which reaches similar efficiencies compared to water splitting. The system is graphically represented in Fig. 2. The energy balance of the vacuum reactor subsystem is

$$\dot{Q}_{\text{solar,vacuum}} = \dot{Q}_{\text{loss}} + \dot{Q}_{\text{rerad.}} + \dot{Q}_{\text{heat,CeO}_2} + h_{\text{CO}_2}(\dot{n}_{\text{CO}_2,\text{out}} - \dot{n}_{\text{CO}_2,\text{in}}) + \dot{n}_{\text{O}_2} h_{\text{O}_2} + \dot{n}_{\text{CO}} h_{\text{CO}} \quad (1)$$

and of the inert gas reactor subsystem

$$\dot{Q}_{\text{solar,inertgas}} = \dot{Q}_{\text{loss}} + \dot{Q}_{\text{rerad.}} + \dot{Q}_{\text{heat,CeO}_2} + h_{\text{CO}_2}(\dot{n}_{\text{CO}_2,\text{out}} - \dot{n}_{\text{CO}_2,\text{in}}) + \dot{n}_{\text{O}_2} h_{\text{O}_2} + \dot{n}_{\text{inertgas}}(h_{\text{inertgas,out}} - h_{\text{inertgas,in}}) + \dot{n}_{\text{CO}} h_{\text{CO}} \quad (2)$$

The solar power input to the vacuum reactor can be written as

$$\dot{Q}_{\text{solar,vacuum}} = \frac{1}{\eta_{\text{abs}}}(\dot{Q}_{\text{heat,CeO}_2} + \dot{Q}_{\text{red,CeO}_2} + \dot{Q}_{\text{heat,CO}_2} + \dot{Q}_{\text{loss}} - \dot{Q}_{\text{products}}). \quad (3)$$

and for the inert gas reactor

$$\dot{Q}_{\text{solar,inertgas}} = \frac{1}{\eta_{\text{abs}}}(\dot{Q}_{\text{heat,CeO}_2} + \dot{Q}_{\text{red,CeO}_2} + \dot{Q}_{\text{heat,CO}_2} + \dot{Q}_{\text{loss}} - \dot{Q}_{\text{products}} + \dot{Q}_{\text{heat,inertgas}}) \quad (4)$$

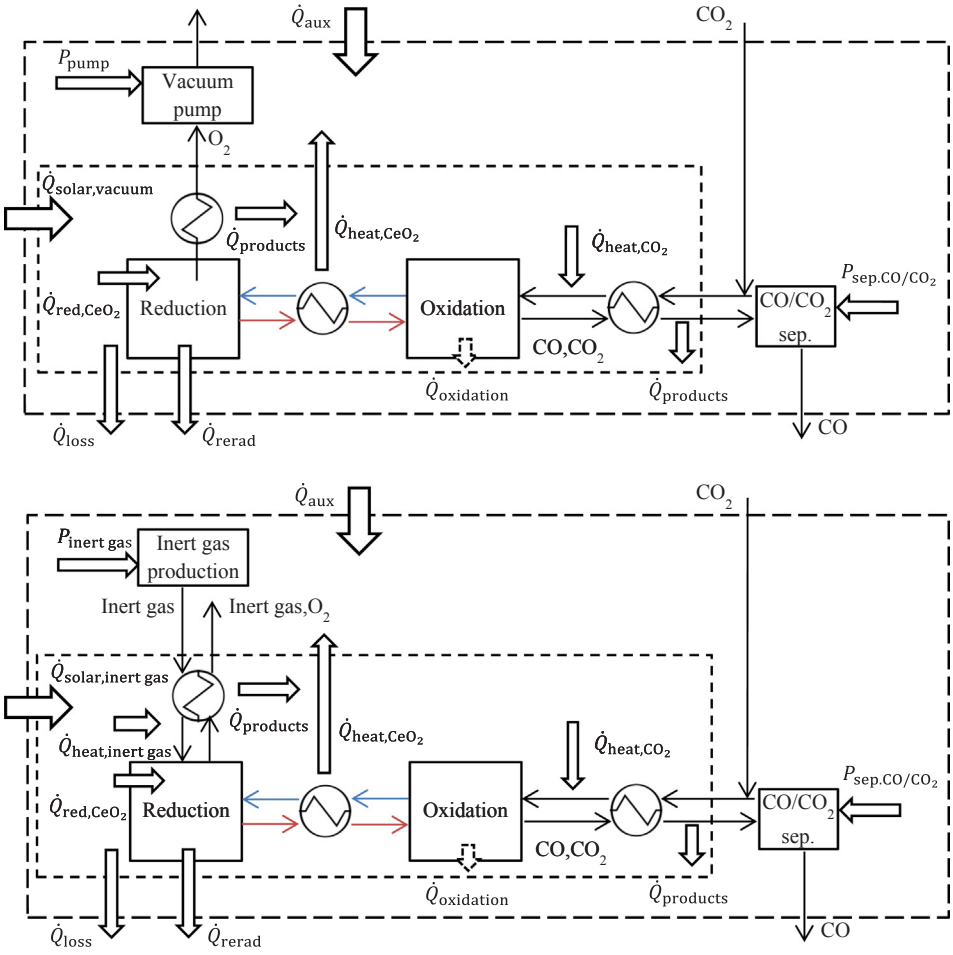

Fig. 2. Schematic of thermochemical conversion including energy flows (thick arrows) and mass flows (thin arrows). (a) Reactor operated under vacuum, (b) reactor operated with inert gas flow.

η_{abs} is the absorption efficiency of the solar reduction chamber and is, assuming a well-insulated blackbody cavity, $\eta_{abs} = 1-\frac{\sigma T^4}{I \cdot C}$. I is the intensity of solar radiation and C the concentration efficiency which are assumed to be 1 kW m^{-2} and 3000 suns, respectively. Reradiation can be calculated from

$$\dot{Q}_{rerad} = (1-\eta_{abs})\cdot\dot{Q}_{solar} \tag{5}$$

The reactor is further assumed to lose heat by convection and conduction. These losses are expressed by the loss factor F (Bader et al., 2013; Lapp, 2013), which is the fraction of absorbed heat in the reactor which is lost by convection and conduction.

$$\dot{Q}_{loss} = F(\dot{Q}_{solar}-\dot{Q}_{rerad}), \tag{6}$$

$\dot{Q}_{heat,CeO_2}$ is the solar power required to raise the temperature of the oxidized ceria element from the temperature achieved at the exit of the heat exchanger $T_{he,end}$ to the reduction temperature T_H,

$$\dot{Q}_{heat,CeO_2} = (1-\varepsilon_{he})\dot{n}_{CeO_2}\int_{T_L}^{T_H} c_{p,CeO_2}(T)\mathrm{d}T = \dot{n}_{CeO_2}\int_{T_{he,end}}^{T_H} c_{p,CeO_2}(T)\mathrm{d}T, \tag{7}$$

with the heat exchanger effectiveness ε_{he}.

$\dot{Q}_{red,CeO_2}$ is the power required to reduce the material from δ_{ox} toδ_{red}

$$\dot{Q}_{red,CeO_2} = \dot{n}_{CeO_2}\Delta H_{red} = \dot{n}_{CeO_2}\int_{\delta_{ox}}^{\delta_{red}} \Delta H_{CeO_2}(\delta)\mathrm{d}\delta. \tag{8}$$

The reduction enthalpy ΔH_{CeO_2} is only slightly dependent on temperature and pressure and is thus modeled to be a function of non-stoichiometry only (Ermanoski et al., 2013).

$\dot{Q}_{heat,CO_2}$ is the thermal power required to heat CO_2 from ambient temperature to the oxidation temperature

$$\dot{Q}_{heat,CO_2} = \dot{n}_{CO_2,in}\int_{T_0}^{T_L} c_{p,CO_2}(T)\mathrm{d}T. \tag{9}$$

The properties of CO_2 and all other gases are calculated with tables from the Engineering Toolbox (2015) and from the VDI Heat Atlas (Kleiber and Joh, 2013).

$\dot{Q}_{heat,inertgas}$ is the net energy required to heat the inert gas from ambient temperature to the reduction temperature

$$\dot{Q}_{heat,inertgas} = (1-\varepsilon_{gasrec})\dot{n}_{inertgas}\int_{T_0}^{T_H} c_{p,inertgas}(T)\mathrm{d}T, \tag{10}$$

where the inert gas is assumed to be nitrogen and heat recuperation from the hot inert gas coming from the reduction reactor is taken into account.

$\dot{Q}_{products}$ is the thermal power which is recovered with an effectiveness of ε_{gasrec} from gases leaving the reduction and oxidation reactions (O_2, CO, CO_2).

$$\dot{Q}_{Products} = \varepsilon_{gasrec}\left(\dot{n}_{CO}\int_{T_0}^{T_L} c_{p,CO}(T)\mathrm{d}T + \dot{n}_{CO_2,out}\int_{T_0}^{T_L} c_{p,CO_2}(T)\mathrm{d}T\dot{n}_{O_2}\int_{T_0}^{T_L} c_{p,O_2}(T)\mathrm{d}T\right) \tag{11}$$

In the calculations, the following requirement is met for all operating points $\dot{Q}_{Products} \le \dot{Q}_{heat,CO_2}$. Mechanical energy which is required to move ceria is neglected as it is small compared to the heating value of the produced syngas. At this point, the energy released during the exothermic oxidation of ceria is not assumed to be recovered.

The vacuum pump power is

$$P_{pump} = \frac{\dot{n}_{O_2}\mathscr{R}T_{pump}\ln\left(\frac{p_0}{p_{O_2}}\right)}{\eta_{pump}}, \tag{12}$$

where the vacuum pump efficiency η_{pump} is taken from a recent analysis (Brendelberger et al., 2017) of screw pumps, roots pumps and turbo pumps in configurations of up to four stages. The authors propose a model for the description of the pump power and efficiency which is validated with data from a manufacturer. The resulting pumping efficiencies are 26.2% at 1000 Pa in the reactor, 13.5% at 100 Pa and 4.6% at 10 Pa. The choice of reactor pressure is thus a trade-off towards lower pressures between decreasing pump efficiency and enhanced productivity of the redox cycle due to the increased nonstoichiometry of ceria at lower oxygen partial pressures (Panlener et al., 1975).

Alternatively to vacuum pumping, the oxygen partial pressure may be reduced by flushing the reactor with an inert gas such as argon or nitrogen, as used in recent experiments for the production of solar syngas (Marxer et al., 2015a, 2017; Chueh et al., 2010; Furler et al., 2012). The evolving oxygen is diluted and removed from the reaction zone by the inert gas, where the dominant mechanism is dependent on the reactor and flow configuration. The reactor configuration, the operating conditions, the morphology of the reactive material, and the properties of the gas flow, besides others, determine the required amount of inert gas that is needed to establish a certain oxygen partial pressure in the reactor. The exact amount will therefore depend on many variables and operating conditions and it is difficult to make a general statement which is valid for a variety of concepts. Nevertheless, a higher and lower bound of the quantity of inert gas needed can be found which is helpful for the assessment of reactor concepts based on the use of vacuum pumping and inert gas flushing. In the recent literature, the inert gas demand has been estimated in different ways, e.g. the perfect mixing of evolving oxygen and inert gas (Ermanoski et al., 2013) or a perfect counter flow of reactive material and inert gas (Bader et al., 2013), leading to significantly different results. Brendelberger et al. (2015) discuss these different approaches and derive a more realistic quantity of inert gas for a counter-flow configuration between reactive material and gas. By taking into account the coupled characteristics of oxygen release from the material and the change of oxygen partial pressure in the surrounding gas, an expression for the inert gas flow rate is found. The required gas quantity can be further reduced if the reduction reaction is not allowed to reach its final state but if the reaction is stopped at an earlier point, i.e. at a reduction extent which is lower than the maximum possible considering the oxygen partial pressure of the incoming gas stream. To achieve a final reduction extent of $\delta = 0.02$ corresponding to an oxygen partial pressure of 1000 Pa at a reduction temperature of 1800 K, the ratio of inert gas to evolving oxygen is $n_{inert}/n_{O_2} = 15$ (Brendelberger et al., 2015). The energy penalty associated with the production of inert gas is $E_{inertgas} = 16\,kJ_{el}\,mol^{-1}$ (Häring and Ahner, 2008) and the corresponding electrical power input $P_{inertgas} = \dot{n}_{inertgas}\cdot E_{inertgas}$.

The oxygen flow rate $\dot{n}_{O_2}$ is derived from the stoichiometry of the overall reaction as half of the carbon monoxide flow rate, the pump temperature T_{pump} is assumed to be the ambient temperature and p_{O_2} is the partial pressure of oxygen during reduction.

The CO/CO_2 separation is assumed to be complete, i.e. pure streams of CO and CO_2 are produced. Literature data for the CO_2 capture from a flue gas stream of a fossil power plant are chosen as a reference (Zeman, 2007), where 132 kJ of heat and 9 kJ of electricity are required for the capture of one mol of CO_2. The auxiliary electrical power input consists of the reduction of the oxygen partial pressure either through vacuum pumping or inert gas sweeping, and the separation of the CO/CO_2 mixture, $P_{aux,vacuum} = P_{pump} + P_{sep,CO/CO_2}$ or $P_{aux,inertgas} = P_{inertgas} + P_{sep,CO/CO_2}$. P_{aux} is then divided by the conversion efficiency of heat to electricity $\eta_{heat-to-electricity}$to arrive at the auxiliary thermal power input

$$\dot{Q}_{aux} = \frac{P_{aux}}{\eta_{heat-to-electricity}}$$

The efficiency of the reactor is defined as

$$\eta_{reactor} = \frac{\text{chemical energy stored in product}}{\text{solar power into reactor + auxiliary power}} = \frac{\dot{n}_{CO} HHV_{CO}}{\dot{Q}_{solar} + \dot{Q}_{aux}}. \quad (13)$$

The efficiencies of splitting water and carbon dioxide deviate only slightly and the efficiency of the latter is used as representative for the reactor operation.

2.2. Thermochemical energy conversion efficiency

For the determination of thermochemical cycle efficiency, in a baseline case we assume (see Table 1) a reduction and oxidation temperature of 1800 K and 1000 K, an oxidation pressure of 1 atm, a concentration ratio of 3000 suns, a CO_2 flow rate during oxidation which corresponds to twice the amount minimally needed to fully reoxidize the material, a heat recuperation of 50% from the solid and fluid phases, and a heat loss factor of 0.1. Electricity is assumed to be produced from incident sunlight with an efficiency of 20%, which results in a heat-to-electricity efficiency of 38.7% at a solar concentration efficiency of 51.7% (Sargent and Lundy, 2003). The choice of reaction temperatures follows recent experimental work (Chueh et al., 2010; Marxer et al., 2017, 2015b; Furler et al., 2014) and theoretical analyses of the ceria redox cycle undergoing a temperature swing (Chueh and Haile, 2010; Lapp et al., 2013; Falter et al., 2015b; Bulfin et al., 2015; Krenzke and Davidson, 2015).

The oxygen partial pressure during reduction is chosen to maximize the reactor efficiency, whereas the oxygen nonstoichiometry δ (and thus CO productivity in oxidation) is increased towards low pressures and the energy to establish the reduced pressure is minimized towards high pressures. In case of vacuum operation, the reactor is evacuated and the total pressure of the reactor is equal to the oxygen partial pressure. In case of inert gas operation, on the other hand, the reactor operates at atmospheric pressure but the oxygen partial pressure is reduced by the reduced oxygen content in the inert gas. The optimal reduction pressure is then a trade-off between these two mechanisms and has a value of 2×10^1 Pa for the vacuum reactor and of 4×10^2 Pa for the inert gas reactor (Fig. 3). Towards lower pressures, the energy penalty of the pumping and inert gas production starts dominating and reduces efficiency, and towards larger pressures than the optimum the fuel productivity is lowered, which likewise has a detrimental effect on efficiency. Compared to the analysis by Ermanoski et al. (2013) a similar peak of efficiency for the inert gas reactor is seen, however, shifted to lower reduction pressures between 100 and 1000 Pa (as compared to 1000–10,000 Pa in Ermanoski et al. (2013). The reason is that Ermanoski et al. (2013) assume perfect mixing of oxygen and inert gas, which leads to a large inert gas flow rates. In this study, however, we assume a counter-flow of inert gas and oxygen as in Brendelberger et al. (2015) which significantly reduces the quantity. At a given flow rate of inert gas and thus energy input, the more efficient counter-flow configuration achieves a lower oxygen partial pressure which shifts the maximum efficiency to lower pressures.

For vacuum pumping, the energy demand for the reduction of the oxygen partial pressure is lower than for inert gas sweeping, which allows going to lower partial pressures and achieving higher overall efficiencies. This is also reported in recent experiments (Marxer et al., 2017), where an enhancement of efficiency is attained with i.a. vacuum pumping. For the following calculations, the oxygen partial pressure during reduction is chosen which maximizes efficiency.

Using the assumptions for the baseline case, an energy conversion efficiency of 11.5% is achieved with the vacuum reactor, where the largest energy input is the thermal cycling of the reactive material ceria (Fig. 4). This has been observed by Chueh and Haile (2010) for the case of no heat recovery and by (Falter et al., 2015b) for a heat recuperation effectiveness of over 70%. This is due to the chosen operating conditions, at which ceria is retained in its solid phase and a small oxygen nonstoichiometry is produced in the material. As the nonstoichiometry is on the order of 0.03, only 1.5% of the oxygen atoms take part in the redox reaction and the thermal energy of cycling the material is dominant when compared with reactions which fully reduce the reactive material, such as the zinc oxide cycle. This can be calculated from the energy of heating and reducing the two materials per mol of oxygen released. For an efficient nonstoichiometric cycle, it is therefore required to recuperate the heat which is used for thermally cycling the reactive material as already observed in other publications (Lapp et al., 2012; Allendorf et al., 2008; Ermanoski et al., 2013; Bader et al., 2013). We have assumed a baseline case heat recuperation effectiveness of 50% both from the solid and from the gas phase.

For the vacuum operation, the second largest item of the energy balance is the reduction enthalpy, which has to be supplied by thermal energy to the solar reactor and is slightly larger than the energy for vacuum pumping. At the chosen reduction pressure of 2×10^{-4} atm, the efficiency of vacuum pumping is 6.7% and the associated pumping power is about half of the required energy input for thermal cycling of the reactive material. Towards higher pressures, the efficiency of vacuum pumping can be enhanced, however, at the cost of reduced fuel productivity from the material and overall reduced cycle efficiency. The reduction pressure has been chosen such as to maximize the reactor efficiency, which entails the operation at a less than optimal pumping efficiency. The energy released during the exothermic oxidation reaction is assumed to stabilize the temperature of the reactive material and otherwise to be lost, which may be a conservative assumption considering the possibility for process enhancements. The magnitude of the energy released is on the order of 192 kJ mol^{-1} CO (Marxer et al., 2017) and therefore about equal to the heat equivalent of gas separation. At the high temperatures of 1800 K, the reactor has an absorption efficiency of 80.2% and a significant amount of energy is lost by reradiation. This loss is very difficult to prevent in a continuous reactor concept because any attempt to capture the reradiated energy from the reactor is likely to interfere with the incoming radiation. An exception could possibly be the use of a reflective coating at the inside of the reactor window. Gas separation of CO and CO_2 accounts for a lower energy input, which depends on the amount of oxidant injected during oxidation. Due to thermodynamic and kinetic reasons, the oxidant quantity is chosen larger than the minimum for stoichiometric oxidation. The thermal energy for heating the oxidant CO_2 to the oxidation temperature has only a small influence and the energy recovered from O_2, CO and CO_2, is negligible.

For the case of inert gas operation, the efficiency of the baseline case is 6.8% and the energy balance has a different appearance. Due to the lower productivity of the cycle according to the higher oxygen partial

Table 1
Parameter values for baseline case.

Parameter	Label	Value	Unit
Concentration ratio	C	3000	–
Oxidation temperature	T_L	1000	K
Reduction temperature	T_H	1800	K
Temperature of surroundings	T_0	300	K
Reduction pressure vacuum reactor	p_{red}	2×10^{-4}	atm
Reduction pressure inert gas reactor	p_{red}	4×10^{-3}	atm
Oxidation pressure	p_{ox}	1.0	atm
CO_2-flow (times min = δ_{red}) in oxidation chamber	f_{CO_2}	2.0	–
Effectiveness of solid heat recovery	ε_{he}	50%	–
Effectiveness of gas heat recovery	ε_{gasrec}	50%	–
Heat loss factor	F	0.1	–
Conversion efficiency of heat to electricity	$\eta_{heat-to-electricity}$	0.39	–

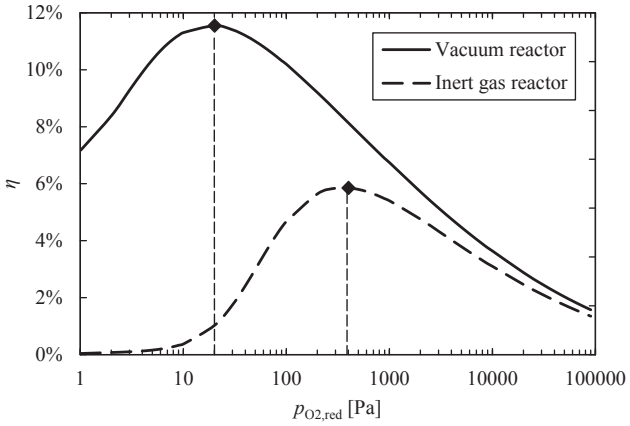

Fig. 3. Thermochemical energy conversion efficiency of vacuum reactor and inert gas reactor. Due to the different energy penalties of establishing the reduced oxygen partial pressure during reduction, the peak of efficiency is shifted between the two concepts (11.5% at 20 Pa for the vacuum reactor and 6.8% at 400 Pa for the inert gas reactor).

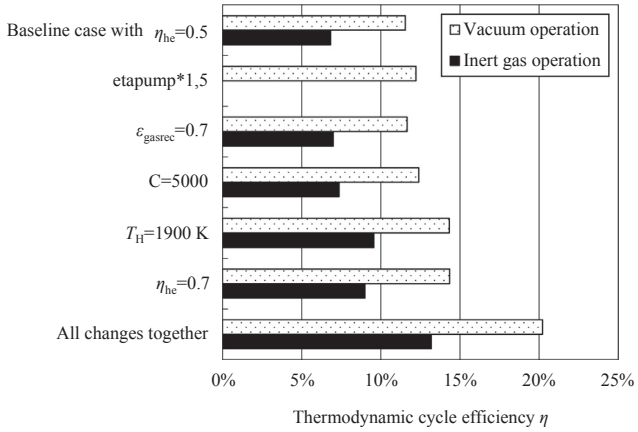

Fig. 5. Enhancement of cycle efficiency of the vacuum reactor and inert gas reactor for a change of selected variables. All other variables are chosen according to the baseline case in Table 1.

pressure, the energies are referenced to a smaller product stream. The specific energy input per mol of CO is then significantly higher than for the case of vacuum pumping, whereas the energy balance is also clearly dominated by the thermal cycling of ceria, as observed for the case of no heat recuperation e.g. by Chueh and Haile (2010). The second largest item is reradiation, where compared to the vacuum reactor the overall thermal power input to the reactor is larger to cover the energy penalties of producing and heating the inert gas, which increases the reradiation losses. The inert gas production and reduction enthalpy have slightly smaller contributions. Heating the inert gas to the reduction temperature requires about half of the energy for its production, whereas 50% of the thermal energy is recuperated. Conduction and convection losses have a small influence on the energy balance, and heating of the oxidant and heat recuperation from the product gases a minor influence.

2.3. Enhancement of thermochemical energy conversion efficiency

The thermochemical energy conversion efficiency describes the fraction of the energy input (concentrated solar energy and auxiliary energy) which is converted into syngas. It therefore defines the size of the solar concentrator, as a more efficient solar reactor will require a smaller power input to produce the same amount of syngas. The heliostat field represents the largest cost item for CSP tower plants (Hinkley et al., 2011; International Energy Agency, 2010) which is likely to be the case also for tower plants for the production of hydrocarbon fuels (Falter et al., 2016). The economics of solar fuel production are therefore crucially dependent on the thermochemical energy conversion efficiency. A thermochemical energy conversion efficiency of 11.5% or less as derived for the baseline case is unlikely to allow production costs which are competitive with conventional fuels or the best alternative fuels. As indicated in a recent study, an efficiency of about 20% is expected to be required, which is also confirmed by economic studies (Falter et al., 2016; Stechel and Miller, 2013; Kim et al., 2012). It is therefore of high importance to increase the conversion efficiency of the solar reactor. In the following, based on the system presented above and on latest findings in the literature on energy requirements of vacuum pumping and inert gas flow rates, we present possibilities for the enhancement of the thermochemical energy conversion efficiency by selectively changing single or multiple variables (Fig. 5) in the framework introduced above. By including energy requirements for the reduction of i.a. oxygen partial pressure and gas separation, and basing them on realistic assumptions, we try to give a reasonable estimation of efficiencies. For the vacuum reactor, we increase the gas heat recuperation effectiveness to 70% as values of even up to 95% have been shown to be achievable (Bader et al., 2013), which however increases the efficiency only to 11.7%. As the energy associated with heating and cooling gases only has a small influence, the increase of recuperation effectiveness equally has a limited effect. In the

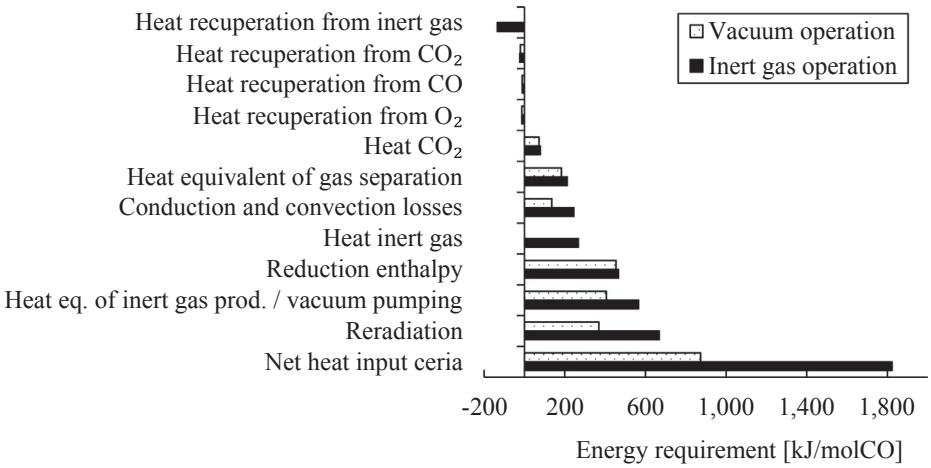

Fig. 4. Energy balance of solar thermochemical CO production in vacuum reactor and inert gas reactor using the assumptions of the baseline case. At an effectiveness of solid heat recovery of 50%, the energy input for heating the reactive material ceria still represents the largest item of the balance.

baseline case, a concentration ratio of 3000 suns has been assumed which may be approached by a solar tower with a secondary concentrator. When moving to a concentrator with even better optics and a concentration ratio of 5000 suns, reradiation losses are decreased and the cycle efficiency improves to 12.4%. A similar effect is achieved if the efficiency of vacuum pumping is increased by 50% to 10.1%. Even though vacuum pumping requires a significant amount of energy, its share in the energy balance is below 20% and therefore its influence is limited. Another important variable is the upper process temperature which, together with the oxygen partial pressure, determines the oxygen nonstoichiometry of the reactive material and thus the amount of CO or syngas produced. Upon an increase from 1800 K to 1900 K, the cycle efficiency rises to 14.3%. At elevated temperatures, losses by reradiation increase. However, the effect of enhanced fuel production outweighs this effect for the indicated temperature increase. Towards even higher temperatures, there exists a theoretical maximum temperature for which the efficiency of the cycle is maximized, balancing reradiation losses and fuel production. Above this temperature, reradiation losses start dominating the energy balance and efficiency decreases again. In general, this temperature is unlikely to be reached in reality as there are constraints with respect to the stability of the materials (Furler et al., 2012; Miller et al., 2014). In a recent experiment, however, a temperature of 1873 K was reached (Furler et al., 2012), whereas it remains to be explored whether these and more severe conditions can be upheld in a constant operation of the reactor.

If 70% of the energy for thermally cycling the reactive material can be recuperated, the cycle efficiency is enhanced to 14.4%. This result is expected since the largest contribution in the energy balance is heating ceria. From an experimental point of view, the implementation of a heat exchanger with an effectiveness of 50% or even 70% certainly represents a challenge. Nevertheless, theoretical analyses of new concepts have demonstrated that such a performance is in principle possible and thus it is the measure with the single largest effect on the cycle efficiency. However, to reach 20% cycle efficiency the discussed measures have to be combined which increases the efficiency from 11.5% to 20.2%.

The general observations seen for the vacuum reactor hold also for the inert gas reactor, with a limited influence of increased gas recuperation effectiveness and concentration ratio. For a significant improvement, an elevation of the reduction temperature and of the solid heat recuperation effectiveness is required, where the maximum efficiency is 13.2%, given that all changes can be implemented at the same time.

The achievement of 20% cycle efficiency, as thought to be required for an economically competitive process, is thus only possible for the vacuum reactor under the assumption that further process enhancements can be made. These enhancements should include an increase of the reduction temperature and of the solid heat recuperation effectiveness.

3. Solar thermochemcial fuel pathway

3.1. System efficiency

To gain a better understanding of the implications of the thermochemical efficiency on the overall solar hydrocarbon production from sunlight, water and carbon dioxide, the system boundary is widened to include resource provision, solar concentration, and hydrocarbon synthesis from synthesis gas produced in the solar thermochemical reactors. Due to its higher efficiency, vacuum operation is chosen for the reactors with a reduction temperature of 1900 K, a 50% enhanced vacuum pumping efficiency, a solid and gas heat recuperation effectiveness of 70%, respectively, and a solar concentration ratio of 5000 suns, resulting in a thermochemical cycle efficiency of 20.2% for CO_2 splitting and 21.6% for the combined H_2O and CO_2 splitting, whereas the higher efficiency is due to a decreased energy input for product gas splitting.

To determine the efficiency of the fuel production system, the produced chemical energy (LHV of the functional unit of 1 L jet fuel and 0.87 L naphtha) is divided by the energy required for its production, consisting of resource provision, solar concentration, thermochemistry, and syngas conversion. A common basis of thermal energy is chosen

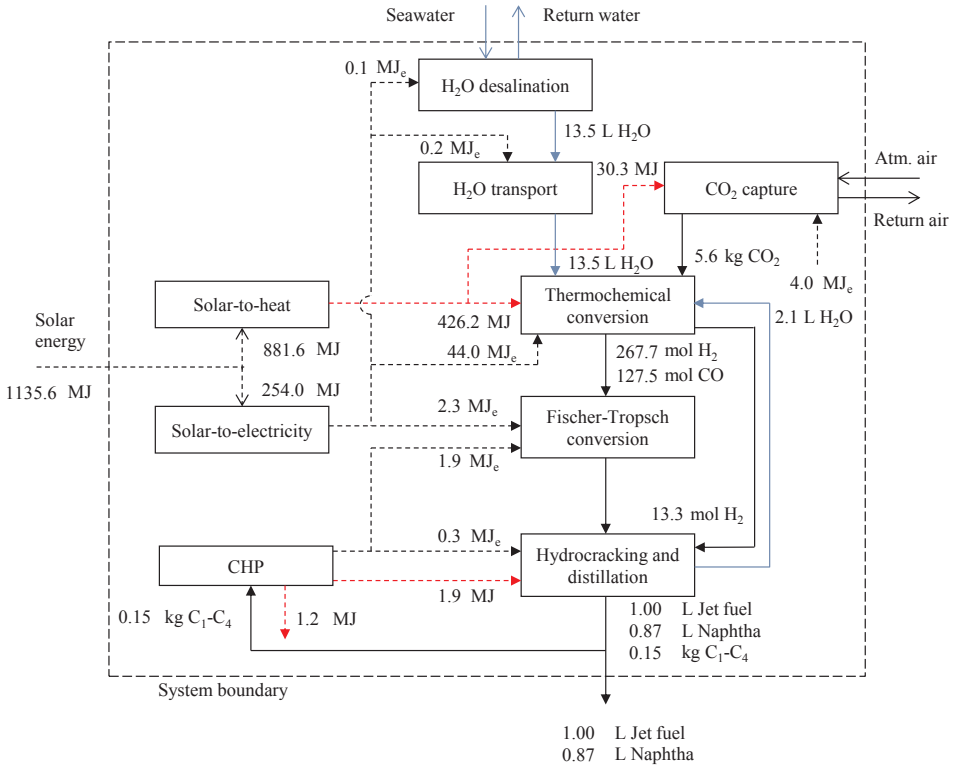

Fig. 6. Energy and mass balance of solar thermochemical fuel plant operating with a vacuum reactor at a thermochemical energy conversion efficiency of 21.6% (concentrated sunlight to syngas). The values are normalized to the output of one functional unit, i.e. 1 L jet fuel and 0.87 L naphtha. Dashed lines represent energy flows and solid lines material flows.

and electrical energy is converted from heat with an efficiency of 38.7%. In the following, the derivation of the energy demand is presented.

The energy and mass balance for a solar thermochemical fuel production plant using a vacuum reactor is shown in Fig. 6, where the values are normalized to the production of one functional unit (1 L jet fuel and 0.87 L naphtha).

1.1 GJ of solar energy is converted to heat (78% of primary energy) and electricity (22%) then used in the fuel production process. Most of the energy drives the thermochemical conversion that requires heat for the thermal cycling and the reduction of ceria, the heating of the reactants, heat losses and the separation of CO and CO_2, and electricity for the gas separation and vacuum pumping. The energy requirement of water desalination and transport is negligible, for CO_2 capture however significant, but below 10% of the energy demand of the thermochemical conversion. The Fischer-Tropsch refining steps require the input of heat and electricity on a low level, where the light hydrocarbon fraction is combusted in a combined heat and power plant (CHP) and the resulting energy is reused in the process. 1.2 MJ of heat is lost from the CHP plant. In the following the process steps are discussed in more detail.

Carbon dioxide is captured from the atmosphere via chemical adsorption to an amine-functionalized sorbent at a specific energy demand of 1500 $kWh\,t^{-1}$ of heat and 200 $kWh_{el}\,t^{-1}$ of electricity (Climeworks, 2014). The largest part of the energy requirement is covered by low-temperature heat to desorb CO_2 from the sorbent, which can frequently be provided in industrial processes as a waste stream otherwise lost to the environment. Furthermore, transport of CO_2 over long distances is avoided because the capture plant can be built at the site of the fuel production plant. Under the assumption of an Anderson-Schulz-Flory distribution in combination with a carbon efficiency of 90% in the Fischer-Tropsch (FT) conversion, 127.49 mol or 5.6 kg of CO_2 are required for the production of one functional unit (1 L jet fuel and 0.87 L naphtha), if an output of 50% jet fuel, 40% naphtha and 10% light hydrocarbons is achieved. Water is provided by seawater desalination from a plant located at the sea at 500 km distance and 500 m altitude difference with respect to the fuel production plant. The desalination plant operates based on reverse osmosis with an energy requirement of 3 $kWh_{el}\,m^{-3}$ water (Elimelech and Phillip, 2011). The energy requirement for pipeline transport of water to the fuel plant is calculated based on Milnes (2013). The water consumption is comprised of contributions for thermochemical conversion of water to hydrogen (for syngas production and hydrocracking of long-chained FT products), cleaning the mirrors of the heliostat field and the water demand for the production of CSP electricity on-site. For the derivation of the specific water demand of mirror cleaning and CSP electricity, the findings of a recent life cycle study are used (Whitaker, 2013), and for thermochemistry stoichiometry is assumed, which may be achieved by recycling the excess oxidant supplied to the thermochemical reactors. The external water demand is reduced by the water volume produced on-site in the FT conversion (about 2 L per functional unit). In the case of the vacuum reactor, the direct on-site demand is 13.5 L for the production of one functional unit and is comprised of 42% for mirror cleaning, 36% for CSP electricity, and 22% for thermochemistry. As shown in Falter and Pitz-Paal (2017) the total water footprint is dominated by its indirect components, mainly the production of ceria in rare earth mines. The direct component has a comparably much smaller influence.

The energy for the thermochemical conversion of water and carbon dioxide into syngas is provided by concentrated sunlight and electricity, where the former is provided by a solar tower concentrator and the latter by an adjacent CSP plant. For the determination of the size of the heliostat field of the solar tower, only the required thermal power input to the reactor is used ($\dot{Q}_{solar}$ in Eq. (10)), whereas a location with a direct normal solar irradiation of 2500 $kWh\,m^2\,y^{-1}$, an efficiency of solar concentration of 51.7% for the solar tower and of 20% for the conversion of solar energy to electricity is assumed (Sargent and Lundy, 2003). The thermochemical energy conversion efficiency is 21.6% for the combined splitting of H_2O and CO_2 in a vacuum reactor.

As the FT synthesis operates at elevated pressures, a compression of the syngas coming from the thermochemical reactor to 30 bar is assumed and the corresponding energy demand is calculated from the ideal isothermal compression work with a compression efficiency of 80%. The synthesis reactions in the FT reactor are exothermal and thus do not require the input of energy. The refining of the FT products into jet fuel and naphtha, however, is done via hydrocracking of the long-chained hydrocarbons and distillation of the intermediate products, which requires 1.9 $MJ\,kg_{C5+}^{-1}$ of thermal and 0.2 $MJ_{el}\,kg_{C5+}^{-1}$ of electrical energy (Beiermann, 2007).

The system efficiency of solar fuel production is then derived by dividing the energy content of the products (lower heating value, LHV) by the primary energy required for their production (incident solar energy input to process).

$$\eta_{system} = \frac{\text{chemical energy stored in product}}{\text{solar energy input to process}} = \frac{LHV_{jetfuel} + LHV_{naphtha}}{Q_{primarysolar}}. \quad (14)$$

With the LHV of jet fuel of 33.4 $MJ\,L^{-1}$ (Stratton et al., 2010) and of naphtha of 31.1 $MJ\,L^{-1}$ (Stratton et al., 2010) the system efficiency is then $(33.4\,MJ\,L^{-1} + 0.87 \times 31.1\,MJ\,L^{-1})/1.1356\,GJ = 5.3\%$. Thus 5.3% of the solar primary energy input is converted to chemical energy stored in the fuels. At an ambitious but realistic target for the thermochemical efficiency of slightly above 20%, the overall system efficiency of solar fuel production is therefore about one quarter of this number. Assuming this target can be reached, the other system components and their integration are assessed in the following in the pursuit of an enhancement of efficiency.

3.2. Enhancement of system efficiency through the use of waste heat

The system shown in Fig. 6 is not optimized with respect to the recuperation of waste energy. However, as there are several significant sources of heat loss throughout the system, the efficiency could be enhanced by using the lost energy as an input for other process steps. At a higher pathway efficiency, less solar energy is required and the concentrator can be sized smaller, reducing its dominant economic and significant environmental impact (Falter et al., 2016). In the following, the potential enhancement of system efficiency through the recuperation of waste heat is analyzed.

The required energy inputs to the system, i.e. heat at different temperature levels and electricity, are discussed in the following and shown in Fig. 7, while energy losses are shown in Fig. 8. The results are referenced to the energy content of the products, whereas electrical energy is converted to thermal energy equivalent based on an energy conversion efficiency of 38.7% from heat to electricity. The largest energy input is required for the reduction of ceria, which has to be supplied as heat at temperatures between the oxidation and the reduction temperature. The next largest input is required for thermally cycling the reactive material ceria between the reaction temperatures, whereas a solid heat recuperation effectiveness of 70% is chosen here (compared to 50% in Fig. 4). At an effectiveness below about 55%, this energy input dominates the energy balance, which is due to the comparably small share of material that is taking part in the chemical reaction (for ceria on the order of a few percent), while all of the material has to be thermally cycled. This result is inherent for non-volatile reactions and changes for volatile ones performing stoichiometric reactions with reduced specific thermal energy input per mol of syngas produced. Slightly less electrical energy is required for the establishment of a low oxygen partial pressure in the reduction chamber by vacuum pumping. As was seen from the energy balance of the vacuum

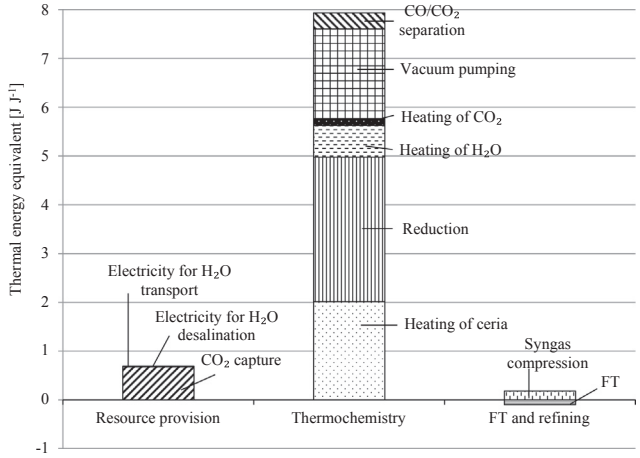

Fig. 7. Energy inputs to solar thermochemical production of 1 L of jet fuel and 0.87 L of naphtha, expressed in thermal energy equivalents. The solid heat recuperation effectiveness is 70%. Electrical energy is converted to thermal energy based on an energy conversion efficiency of 38.7%.

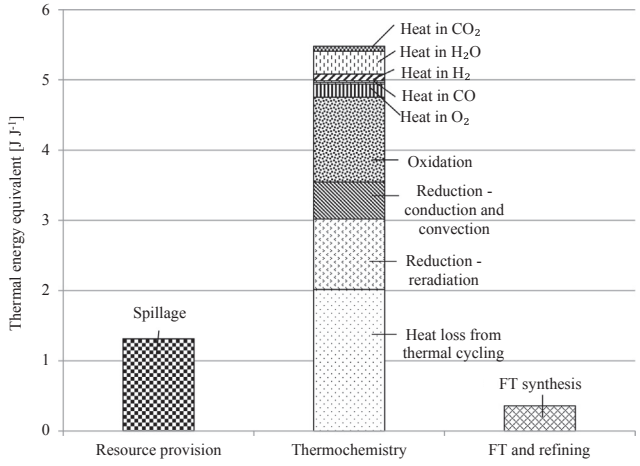

Fig. 8. Energy losses from the solar thermochemical production of 1 L of jet fuel and 0.87 L of naphtha, expressed in thermal energy equivalents. Electrical energy is converted to thermal energy based on an energy conversion efficiency of 38.7%.

reactor above, the choice of pressure level in the reactor has an influence on reactor efficiency through a trade-off of energy requirement and achieved nonstoichiometry, whereas here the pressure is chosen to maximize efficiency. The next largest energy inputs are for CO_2 capture which requires heat at a temperature below 400 K and electricity, H_2O evaporation and heating to the oxidation temperature, and CO/CO_2 separation, which requires heat and electricity. All other energy inputs are comparably small, whereas the Fischer-Tropsch conversion is comprised of the requirements for hydrocracking and distillation and the energy (heat and electricity) gained from the combustion of the gaseous hydrocarbons and has an overall negative value.

Fig. 8 shows the energy losses associated with the production of solar thermochemical fuel. During the concentration of sunlight, energy is lost e.g. by soiling of the mirrors, blocking, shading, cosine losses, atmospheric attenuation, and spillage, where the latter could in theory be recovered by an absorbing cooling device around the reactors. For a tower plant achieving a concentration ratio of 5000 kW m^{-2} with a secondary concentrator, the spillage is derived from the intercept of the reactor and the efficiency of the secondary concentrator and is on the order of 10% of solar primary energy (Pitz-Paal et al., 2011). We are limiting the analysis to tower concentrators due to the significantly different scale-up and field layout of dish concentrators. The largest loss occurs from the thermal cycling of ceria at temperatures between the oxidation (1000 K) and the reduction temperature (1900 K), whereas the required heat input is equal to the energy lost in the heat exchanger between hot and cold material. In other words, a perfect heat exchange between reduced and oxidized material would lead to a value of zero energy lost from thermal cycling and consequently to no required additional thermal energy input. The second largest energy loss from the thermochemical cycle is by oxidation of ceria, whereas this loss occurs within the closed reactor at a temperature of 1000 K and may be used to achieve a steady oxidation temperature or to preheat the oxidants. It is calculated by adding the reaction enthalpies of the reversed reduction and the splitting of water and carbon dioxide, taking into account the different volumes of oxidants. The next largest source is reradiation from the reduction chamber which is at a higher temperature than the surroundings and thus loses heat through its aperture. The recuperation of this energy is very difficult as any capture device operating with continuously irradiated concepts would necessarily block incoming radiation. An exception could be discontinuous concepts such as batch reactors, where the radiation source is only active during reduction and thus reradiation could partly be captured after the reduction step. Another theoretical possibility could be a reflective coating at the inside of the window covering the reduction cavity which is able to reflect infrared radiation. At temperatures and pressures of 1900 K and 2×10^{-4} atm during reduction and 1000 K and 1 atm during oxidation, the reduction enthalpies are 437.1 kJ mol$_O^{-1}$ for water splitting and 436.9 kJ mol$_O^{-1}$ for carbon dioxide splitting. The small difference is attributed to deviating oxygen nonstoichiometries after the respective oxidation reactions, which causes a slightly more complete oxidation of ceria in case of water splitting and therefore a higher energy input for its reduction. The enthalpies of splitting water and carbon dioxide are 247.8 kJ mol$_{H2}^{-1}$ and 283.0 kJ mol$_{CO}^{-1}$ at 1000 K.

Conductive and convective losses from the solar reactors are estimated based on a loss factor of 10% with respect to the absorbed incoming solar energy. Further losses include the energy stored in the product gases of oxygen at the reduction temperature and of CO and H_2 at the oxidation temperature, whereas here this heat is assumed to be captured with an effectiveness of 50%. The Fischer-Tropsch synthesis is exothermic and thus releases heat at a temperature of about 500 K.

For the evaluation of possibilities for heat recovery in the overall process, it is important to take into account the quality of the energy source and sink, i.e. if electricity is required or heat, and at what temperature level in case of the latter. In Figs. 7 and 8, electricity has already been converted to a thermal energy equivalent, making a comparison more easily possible. Assuming that a continuous thermochemical reactor is used, where solar energy is incident on the reduction chamber without interruption throughout the day, the recuperation of reradiation is inherently difficult and thus excluded from the analysis. Assuming further that the heat exchanger is operating at its specified effectiveness and the rest of the energy is lost to the environment, there is no heat source at the required temperature to provide heat to the thermal cycling of ceria besides the oxygen stream leaving the reduction reactor.

Combining the energy demands and losses from the two preceding figures, in Fig. 9, the required inputs to the solar thermochemical fuel production and its losses of heat and electricity are shown (required inputs: positive values, losses: negative values) including the corresponding temperature levels for thermal energy. The largest thermal energy requirements are the reduction of ceria (at 1900 K), the net heat input for its heating to 1900 K (between $T_{he,end}$ and T_H; excluding the energy recuperated in the heat exchanger), the heating of the oxidants to the oxidation temperature, CO_2 capture at 373 K, and the separation of CO and CO_2 at 473 K. Energy is mainly lost through reradiation at 1900 K, through incomplete heat recuperation from the solid phase of the reactive material, the exothermal oxidation reaction at 1000 K, spillage from the concentration of sunlight, conduction and convection losses, and the exothermal Fischer-Tropsch synthesis. The solid-solid

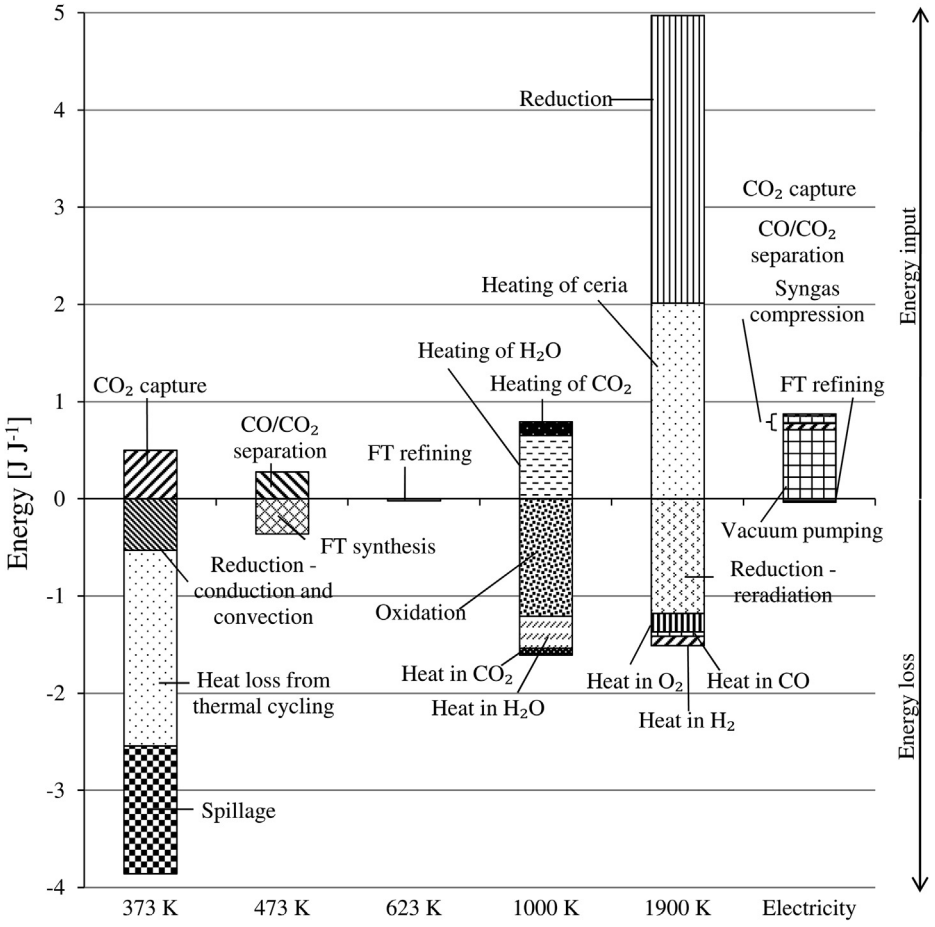

Fig. 9. Combined demands (positive values) and losses (negative values) of heat and electricity from solar thermochemical fuel production based on Figs. 7 and 8. Solid heat recuperation effectiveness is 70%. For thermal energy, the corresponding temperature levels are shown (373–1900 K). The energies are referenced to the lower heating value of the produced fuels and the most important contributions are indicated. The value for "FT refining" is composed of the energy demands for product refining minus the energy derived from the combustion of the gaseous products and has a slightly negative value at a temperature of 623 K and for electricity, whereas "FT synthesis" indicates the exothermal chemical reaction. Heat lost from the thermal cycling of ceria and spillage of solar concentration is assumed to occur at a temperature of 373 K.

heat exchanger operates at an effectiveness of 70% and is assumed to be well-insulated towards the surroundings and thus to lose heat at a comparably low temperature level which depends on its specific implementation (a value of 373 K is chosen here). Electrical energy is required for CO_2 capture, water desalination and transport, CO/CO_2 separation, vacuum pumping, syngas compression, and FT product refining. The small negative values of thermal (at 623 K) and electrical energy derive from the combustion of the light hydrocarbon fraction in a combined heat and power plant.

Given the magnitude of the energy losses from the cycle ($4.9\,J\,J^{-1}$ excluding reradiation) and assuming that these losses can be recuperated with high effectiveness, the energy requirements of CO_2 capture, H_2O desalination and transport, heating of oxidants (H_2O and CO_2), syngas compression, and hydrocracking and distillation of FT products ($3.8\,J\,J^{-1}$) can be covered. The energy conversion efficiency of the overall cycle would then rise from 5.3% to 8.6%. As the losses do not occur in a single place but are distributed over different temperature levels and locations in the process, such as along the heat exchanger, in the oxidation chamber and in the FT synthesis, it is difficult to capture all of the energy with high effectiveness. Nevertheless, this analysis shows that a large potential lies within the recovery of energy losses that occur over the whole process of producing solar thermochemical fuels. As has been shown in previous analyses (Falter et al., 2016; Stechel and Miller, 2013), efficiency of the fuel production pathway is of high importance for the production costs. The use of waste energy to cover heat and electricity demands in the cycle can therefore contribute to a cost reduction, whereas here the additional technical and financial effort for the conversion of waste heat is not analyzed in further detail. The potential that lies within heat recovery is of high importance, since it enables the improvement of the economic and environmental performance of the process without having to increase the conversion efficiency of the thermochemical step. By an efficient design of the fuel production plant, the demanding conditions for the high temperature step may thus be relaxed.

4. Conclusions

The solar thermochemical fuel pathway is analyzed based on a thermodynamic model of the ceria redox cycle. The energy balance and energy conversion efficiencies of the two options for the reduction of the oxygen partial pressure, vacuum pumping and inert gas sweeping, are discussed using the latest published required amounts of inert gas and energy demand for vacuum pumping from the literature. It is found that efficiencies are in general higher for the vacuum reactor due to a lower energy penalty for the establishment of the reduced oxygen partial pressure. To reach energy conversion efficiencies of 20% and above, several operational parameters have to be adjusted. A possible combination requires the following changes from the baseline case: the reduction temperature has to be raised from 1800 K to 1900 K, vacuum pump efficiency has to be raised by 50%, heat recuperation from the gases and the solid phase of the reactive material ceria has to reach an effectiveness of 70%, and the concentration efficiency has to be raised to 5000 suns. While these requirements appear to be very demanding, the analysis of the whole fuel production pathway shows for the first time that the recovery of waste heat from the process holds great potential for the increase of overall fuel production efficiency. If the demands for electricity, low-temperature heat and the heating of the reactants to the oxidation temperature are covered by waste heat, which is shown to be possible in principle, then the pathway efficiency rises by more than 50% from 5.3% to 8.6%. Waste energy from the single process steps can thus significantly enhance solar fuel production through a reduction of production costs and greenhouse gas emissions.

This study therefore represents a first step towards the optimization of integrated solar thermochemical fuel production, which will be of high importance for the technical and economic planning of future plants.

Conflict of interest

There are no conflicts to declare.

Acknowledgements

We gratefully acknowledge the contributions of Arne Roth. The research leading to these results has received funding from the European Union's Horizon 2020 research and innovation program under grant agreement no. 654408.

References

Air Transport Action Group, 2017. Climate Change. <http://www.atag.org/our-activities/climate-change.html> (accessed 8 November 2017).
Allendorf, M.D., Diver, R.B., Siegel, N.P., Miller, J.E., 2008. Energy Fuels 22, 4115–4124.
Axelsson, L., Franzén, M., Ostwald, M., Berndes, G., Lakshmi, G., Ravindranath, N.H., 2012. Biofuels Bioprod. Biorefining 6, 246–256.
Bader, R., Venstrom, L.J., Davidson, J.H., Lipiński, W., 2013. Energy Fuels 27, 5533–5544.
Beiermann, D., 2007. In: DGMK/SCI-Conference, pp. 199–206.
Brendelberger, S., Roeb, M., Lange, M., Sattler, C., 2015. Sol. Energy 122, 1011–1022.
Brendelberger, S., von Storch, H., Bulfin, B., Sattler, C., 2017. Sol. Energy 141, 91–102.
Bulfin, B., Call, F., Lange, M., Lübben, O., Sattler, C., Pitz-Paal, R., Shvets, I.V., 2015. Energy Fuels 29, 1001–1009.
Chueh, W.C., Falter, C., Abbott, M., Scipio, D., Furler, P., Haile, S.M., Steinfeld, A., 2010. Science 330, 1797–1801.
Chueh, W.C., Haile, S.M., 2010. Philos. Trans. A Math. Phys. Eng. Sci. 368, 3269–3294.
Chueh, W.C., Haile, S.M., 2010. Philos. Trans. A. Math. Phys. Eng. Sci. 368, 3269–3294.
Climeworks LLC., 2014. CO2 air capture demonstration plant. <http://www.climeworks.com/co2-capture-plants.html> (accessed 1 June 2014).
Elimelech, M., Phillip, W.A., 2011. Science 333, 712–717.
Engineering Toolbox, 2015. Specific Heat Capacity of Gases. <www.engineeringtoolbox.com> (accessed 30 October 2015).
Ermanoski, I., Siegel, N.P., Stechel, E.B., 2013. J. Sol. Energy Eng. 135, 031002.
Falter, C., Pitz-Paal, R., 2017. Environ. Sci. Technol acs.est.7b02633.
Falter, C., Batteiger, V., Sizmann, A., 2016. Environ. Sci. Technol. 50, 470–477.
Falter, C.P., Pitz-Paal, R., 2017. Sol. Energy 144, 569–579.
Falter, C.P., Sizmann, A., Pitz-Paal, R., 2015b. Sol. Energy. https://doi.org/10.1016/j.solener.2015.10.042.
Falter, C.P., Sizmann, A., Pitz-Paal, R., 2015a. Sol. Energy 122, 1296–1308.
Felinks, J., Brendelberger, S., Roeb, M., Sattler, C., Pitz-Paal, R., 2014. Appl. Therm. Eng. 73, 1006–1013.
Furler, P., Scheffe, J., Gorbar, M., Moes, L., Vogt, U., Steinfeld, A., 2012. Energy Fuels 26, 7051–7059.
Furler, P., Scheffe, J.R., Steinfeld, A., 2012. Energy Environ. Sci. 5, 6098.
Furler, P., Scheffe, J., Marxer, D., Gorbar, M., Bonk, A., Vogt, U., Steinfeld, A., 2014. Phys. Chem. Chem. Phys. 16, 10503–10511.
Goldmann, A., Sauter, W., Oettinger, M., Kluge, T., Schröder, U., Seume, J., Friedrichs, J., Dinkelacker, F., 2018. Energies 11, 392.
Gollakota, A.R.K., Kishore, N., Gu, S., 2018. Renew. Sustain. Energy Rev. 81, 1378–1392.
Häring, H.W., Ahner, C., 2008. Industrial Gases Processing. Wiley - VCH Verlag GmbH & Co. KgaA, Weinheim, Germany.
Hinkley, J., Curtin, B., Hayward, J., Wonhas, A., Boyd, R., Grima, C., Tadros, A., Hall, R., Naicker, K., Mikhail, A., 2011. 1–32.
International Energy Agency, 2010. Technology Roadmap: Concentrating Solar Power. OECD Publishing.
Jarrett, C., Chueh, W., Yuan, C., Kawajiri, Y., Sandhage, K.H., Henry, A., 2016. Sol. Energy 123, 57–73.
Kim, J., Johnson, T., Miller, J.E., Stechel, E.B., Maravelias, C.T., 2012. Energy Environ. Sci. 5, 8417.
Kleiber, M., Joh, R., 2013. VDI-Wärmeatlas, Kapitel D.
König, D.H., Freiberg, M., Dietrich, R.-U., Wörner, A., 2015. Fuel 159, 289–297.
Krenzke, P.T., Davidson, J.H., 2015. Energy Fuels 150206073859007.
Kuhn, H., Sizmann, A., 2012. Deutscher Luft-und Raumfahrt Kongress. DLRK.
Lapp, J., Davidson, J.H., Lipiński, W., 2012. Energy 37, 591–600.
Lapp, J., Davidson, J.H., Lipiński, W., 2013. J. Sol. Energy Eng. 135, 031004.
Lapp, J., 2013. Dissertation. University of Minnesota.
Marxer, D., Furler, P., Scheffe, J., Geerlings, H., Falter, C., Batteiger, V., Sizmann, A., Steinfeld, A., 2015b. Energy Fuels. https://doi.org/10.1021/acs.energyfuels.5b00351.
Marxer, D.A., Furler, P., Scheffe, J.R., Geerlings, H., Falter, C., Batteiger, V., Sizmann, A., Steinfeld, A., 2015a. Energy Fuels 29, 3241–3250.
Marxer, D., Furler, P., Takacs, M., Steinfeld, A., 2017. Energy Environ. Sci. 10, 1142–1149.
Miller, J.E., McDaniel, A.H., Allendorf, M.D., 2014. Adv. Energy Mater. 4, 1300469.
Milnes, M., 2013. The mathematics of pumping water. <http://www.raeng.org.uk/education/diploma/maths/pdf/exemplars_advanced/17_pumping_water.pdf> (accessed 1 January 2013).
Nocera, D.G., 2017. Acc. Chem. Res. 50, 616–619.
Panlener, R.J., Blumenthal, R.N., Garnier, J.E., 1975. J. Phys. Chem. Solids 36, 1213–1222.
Pitz-Paal, R., Botero, N.B., Steinfeld, A., 2011. Sol. Energy 85, 334–343.
Romero, M., Steinfeld, A., 2012. Energy Environ. Sci. 5, 9234.
Sargent & Lundy, 2003. Assessment of Parabolic Trough and Power Tower Solar Technology; SL-5641, Chicago, IL, USA.
Scheffe, J.R., Steinfeld, A., 2012. Energy Fuels 26, 1928–1936.
Schmidt, P., Weindorf, W., Roth, A., Batteiger, V., Riegel, F., 2016. 32.
Stechel, E.B., Miller, J.E., 2013. J. CO_2 Util. 1, 28–36.
Steinfeld, A., Epstein, M., 2001. Chem. Br. 37, 30–32.
Stratton, R.W., Wong, H.M., Hileman, J.I., 2010. Life cycle gas emissions from alternative jet fuels. PARTNER Project 28 report. Report number Partner-Coe-2010-001.
Welte, M., Barhoumi, R., Zbinden, A., Scheffe, J.R., Steinfeld, A., 2016. Ind. Eng. Chem. Res. 55, 10618–10625.
Whitaker, M.B., Heath, G.a., Burkhardt, J.J., Turchi, C.S., 2013. Environ. Sci. Technol. 47, 5896–5903.
Zeman, F., 2007. Environ. Sci. Technol. 41, 7558–7563.